文章编号：1001-9014(2020)05-0576-07

DOI:10.11972/j.issn.1001-9014.2020.05.007

Realization of a multiband metamaterial waveguide based on dirac semimetal in the 800~1100nm range

ZHONG Min[1*], SHI Xian-Chun[2]

(1. Hezhou University, Hezhou 542899, China;
2. School of Mechanical Engineering, Anhui University of Science and Technology, Huainan 232001, China)

Abstract: In this paper, a metamaterial waveguide with four square hole resonators based on Dirac semimetal layers is proposed in the 800~1100nm range. Four transmission peaks (70%, 61%, 72%, and 63%) are achieved at resonance wavelengths 842nm, 921nm, 1010nm, and 1061nm, respectively. These transmission peaks are originated from the interference effect of magnetic fields distributed in the main cavity and cavities 1, 2, 3, or 4. These transmission peaks can be enhanced and moved to shorter wavelengths through increasing the Fermi energy. The proposed metamaterial waveguide can be applied in nanoscale filter, switch, or refractive index sensor.

Key words: metamaterials, transmission, waveguide
PACS: :41. 20. Jb,78. 20. Cj,73. 20. Mf,42. 25. Bs

在800~1100nm范围内实现基于狄拉克半金属的多波段超材料波导

钟 敏[1*], 史先春[2]

(1. 贺州学院,广西 贺州,542899;
2. 安徽理工大学 机械工程学院,安徽 淮南,232001)

摘要:提出了一种基于Dirac半金属层的具有四个方孔谐振器的超材料波导,其波长范围为800~1100nm。在共振波长842nm、921nm、1010nm和1061nm处分别获得四个透射峰(70%、61%、72%和63%)。这些透射峰源自于分布在主腔和腔1、2、3或4中的磁场的干涉增强作用。通过将费米能量从50meV增加到70meV,可以增加四个透射峰并将其转移到更短的波长。所提出的超材料波导可能在纳米级滤波器,开关或折射率传感器中应用。

关 键 词:超材料;传输;波导
中图分类号:O43 **文献标识码**:A

Introduction

Electromagnetic metamaterials reveal many unique properties, which can't be achieved in nature materials, such as, cloaking, negative refraction index, or lensing [1-5]. Based on these unique properties, electromagnetic metamaterials are applied in many areas [6-9]. On the one hand, metamaterial waveguides have attracted the attention of researchers in recent years. Many metamaterials-based waveguides are proposed and verified, including combiner, Mach-Zennder interferometer, or sensor [10-15]. On the other hand, surface plasmon polariton (SPP) mode is revealed by the coupling effect of incident light waves with free electrons on the metal surface. The SPP mode is always propagated forward at the metal-dielectric interface [16-17]. The SPP mode can be excited in metal-dielectric-metal (MDM) electromagnetic metamaterials-based waveguides [18]. The magnetic field resonance ef-

Received date: 2019-12-22, **revised date**: 2020-02-08 **收稿日期**:2019-12-22,**修回日期**:2020-02-08
Foundation items: Supported by the Doctor's Scientific Research Foundation (HZUBS201503), the Young and Middle Teachers' Basic Ability Improvement Project of Guangxi (KY2016YB453), the Mathematical Support Autonomous Discipline Project of Hezhou University (2016HZXYSX01), and the Innovation and Entrepreneurship Students Project of Hezhou University (201611838018, 201911838062, 201911838071, 201911838179).
Biography: Zhong Min (1982-), male, Hezhou, lecturer. Research area involves Metamaterials, Dirac semimetals, Weir semimetals, graphene, phase change materials, sensors. E-mail: zhongmin2012hy@163.com.
* **Corresponding author**: E-mail: zhongmin2012hy@163.com

fect generated in electromagnetic metamaterials-based waveguide is extremely sensitive to environmental changes, which is always applied in sensing, optical switching, or slow light. Many researchers have proposed different metamaterial waveguide designs. For example, Fu *et al* proposed a metamaterial waveguide with cross rectangular cavity, which achieved two narrow-spectrum modes by the rectangular cavity. Moreover, the resonance properties are controlled by changing the length or height of this cross-shaped rectangular cavity [19]. Li *et al* designed a metamaterial waveguide based on the Fano resonances [20]. Chen *et al* suggested a metamaterial waveguide with a rectangular cavity, which revealed two Fano resonance modes, and both modes can be controlled by changing structural parameters [21]. Li *et al* verified a metamaterial waveguide with disc cavity and toroidal cavity [22]. These reported metamaterial waveguides are made of precious metals, causing significant energy loss in electromagnetic waves. At the same time, resonance behaviors of these waveguides can only be modulated by changing the structural parameters, which is not conducive to industrial applications. Therefore, the search for non-precious metal to prepare tunable metamaterial waveguides has become the focus of researchers. Many novel metamaterial waveguides have been designed and verified. For example, *Ouyang et al* verified a tunable metamaterial waveguide with hetero cavities based on the Fano resonance [23]. *Zheng et al* designed and theoretically analyzed a metamaterial waveguide in mid-infrared [24]. Yi *et al* proposed and simulated a tunable MDM waveguide, which could be controlled by changing the refractive indices [25].

In this paper, a tunable MDM waveguide based on Dirac semimetal layers is designed and simulated in the 800~1100nm range. This waveguide reveals four transmission peaks. These transmission peaks are excited by the interference effect between the main cavity and cavities 1, 2, 3, or 4. Since the dielectric constant of Dirac semimetal is sensitive to Fermi energy, resonance wavelenths of transmission peaks can be modulated by changing the Fermi energy. Therefore, the tenability of this waveguide is verified in the 800~1100nm range.

1 Design and model

The proposed metal – insulator – metal waveguide is shown in Fig 1. A reflecting layer is added in the main cavity of the waveguide, which plays as a waveguide modulator. Detailed structural parameters are given in table 1. In this unit cell, two Dirac semimetal layers are described as follows [26]:

$$\mathrm{Re}\sigma(\Omega) = \frac{gk_F e^2}{24\pi\hbar}\Omega G\left(\frac{\Omega}{2}\right) \quad , \quad (1)$$

$$\mathrm{Im}\sigma(\Omega) = \frac{gk_F e^2}{24\pi^2\hbar}\left\{\frac{4}{\Omega}\left[1+\frac{\pi^2}{3}\left(\frac{T}{E_F}\right)^2\right] + 8\Omega\int_0^{\varepsilon_c}\left[\frac{G(\varepsilon)-G(\Omega-2)}{\Omega^2-4\varepsilon^2}\right]\varepsilon d\varepsilon\right\} \quad , \quad (2)$$

where, $E_F$is set to be Fermi level, $k_F = E_F/\hbar v_F$is set to be Fermi momentum, Fermi velocity stands for $v_F = 10^6 m/s$. Moreover, the permittivity of two Dirac semimetal layers is given as follows [27]:

$$\varepsilon = \varepsilon_b + \mathrm{i}\sigma/\omega\varepsilon_0 \quad . \quad (3)$$

Based on the reported work [28], dispersion equation of SPP modes is given as follows in this metal – insulator – metal waveguide:

$$\frac{\varepsilon_o p}{\varepsilon_m k} = \frac{1-\exp(kd)}{1+\exp(kd)} \quad , \quad (4)$$

$$k = (\beta^2 - \varepsilon_o k_o^2)^{1/2} \quad , \quad (5)$$

$$p = (\beta^2 - \varepsilon_m k_o^2)^{1/2} \quad . \quad (6)$$

In the equation above, propagation constant of SPP modes is set to be β. Ideal boundaries are set based on the reported work [29].

Table 1 Geometric parameters

表1 几何参数

Parameter	*P*	*w1*	*L1*	*L2*	*L3*	*L4*	*w2*	*w3*
Value(nm)	300	30	140	140	110	150	80	12

2 Results and discussion

The simulated transmission spectrum of the proposed metamaterials waveguide is shown in Fig 2(b), see the black line. Four transmission peaks are achieved at resonance wavelengths 842nm, 921nm, 1010nm, and 1061nm, respectively. The amplitudes of these transmission peaks are: 70%, 61%, 72%, and 63%, respectively. This waveguide reveals multi-band transmission behaviors. For ease of description, these transmission peaks are labeled as: P1, P2, P3, and P4, respectively. It is found that the P1 and P3 are higher than the P2 and P4. These transmission peaks are all narrow bands.

In order to reveal the physical mechanism of these transmission peaks, magnetic field intensity distributions are calculated separately at the resonance wavelengths. For the P1 peak, magnetic field intensity distribution is calculated at resonance wavelength 842nm, as shown in Fig 3(a). It is found that the simulated magnetic field is mainly distributed in the main cavity and the Cavity 1. In contrast, there is substantially no magnetic field distributed in the cavities 2, 3, and 4. Moreover, the magnetic field distributed in the main cavity is coupled with that in the Cavity 1, which results in the P1, as shown in Fig 2(a). In order to better explain the effect of the coupling between different cavities on transmission peaks, the phase spectrum of the proposed metamaterials waveguide is also calculated, as shown in Fig 5. Four phase values close to zero are achieved at resonance wavelengths 842nm, 921nm, 1010nm, and 1061nm. For the P1 peak, the phase value is 0.04. When the electromagnetic wave in the main cavity is coupled with that in the Cavity 1, the phase value is close to zero, which results in the enhancement of the transmission, as shown in Fig 3(a). In contrast, when the calculated wavelength is deviated from the resonance wavelength, the transmission

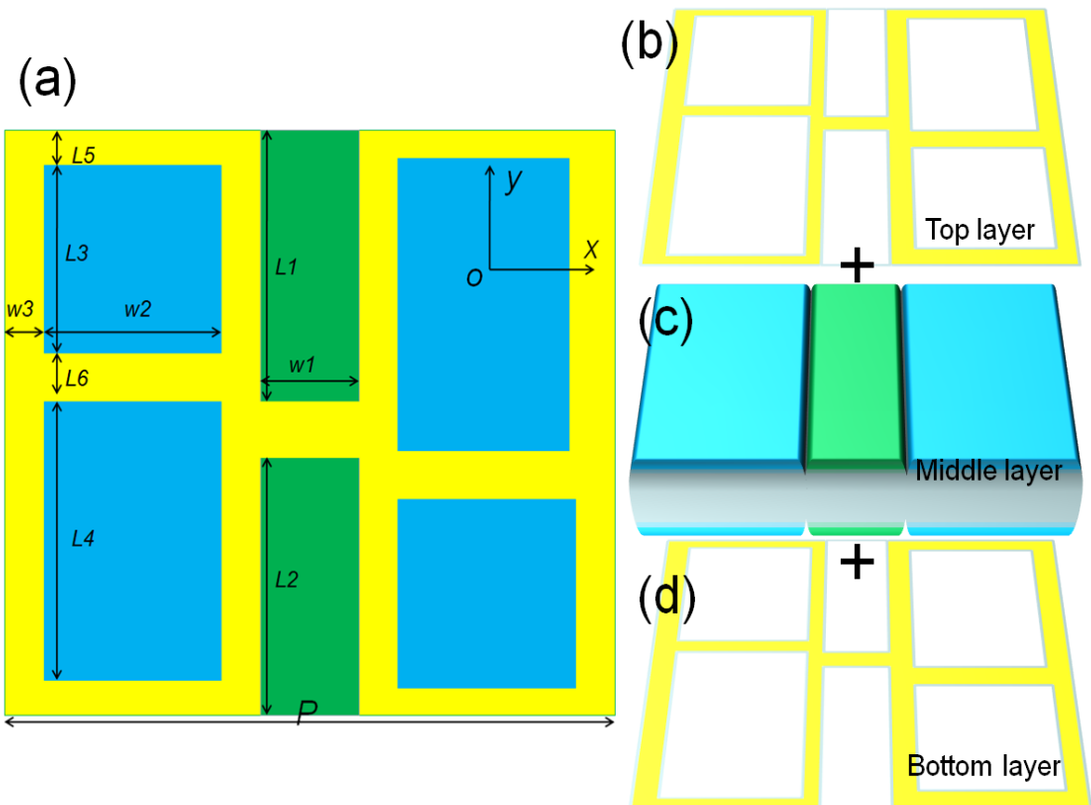

Fig 1 (a) Schematic diagram of the proposed metal – insulator – metal waveguide. The yellow parts are Dirac semimetal layers. The green part is SU-8 layer. The blue part is SiO_2. (b) The top layer of the proposed unit cell. (c) The middle layer of the proposed unit cell. (d) The bottom layer of the proposed unit cell. The thickness of SU-8 layer and SiO_2 layer is set as 180nm

图1 (a)金属-绝缘体-金属结构单元的结构示意图,黄色部分是狄拉克半金属,绿色部分是SU-8层,蓝色部分是SiO_2层(b)结构单元的顶层(c)结构单元的中间层(d)结构单元的底层,SU-8层和SiO_2层的厚度都设置为180nm

of the electromagnetic wave is reduced obviously, as shown in Fig 2(b). At the same time, the magnetic field intensity is mainly distributed in the main cavity due to the strong interference conditions are destroyed, as shown in Fig 3(c). In order to better understand the relationship between the coupling resonance behavior and the transmission peak, the transmission spectrum of this waveguide is calculated based on the coupled mode theory. The transmission amplitudes of the main cavity and the Cavities 1, 2, 3, and 4 are set to be A, B, C, D, *and* E. These transmission amplitudes can be defined as follows [30]:

$$\frac{dA}{dt} = k_{e1}S_1 + k_{e2}S_2 + k_{e3}B + k_{e4}C + k_{e5}D + k_{e6}E + [j\omega_A - k_{o1}^2 - k_{e1}^2 - k_{e2}^2 - k_{e3}^2 - k_{e4}^2 - k_{e5}^2 - k_{e6}^2] \times A, \quad (7)$$

$$\frac{dB}{dt} = (j\omega_B - k_{o2}^2 - k_{e3}^2)\cdot B + k_{e3}A, \quad (8)$$

$$\frac{dC}{dt} = (j\omega_C - k_{o3}^2 - k_{e4}^2)\cdot C + k_{e4}A, \quad (9)$$

$$\frac{dD}{dt} = (j\omega_D - k_{o3}^2 - k_{e5}^2)\cdot D + k_{e5}A, \quad (10)$$

$$\frac{dE}{dt} = (j\omega_D - k_{o4}^2 - k_{e6}^2)\cdot E + k_{e6}A, \quad (11)$$

where, ω_A, ω_B, ω_C, ω_D, and $\omega_E$are set to be the resonant frequencies of the main cavity, and cavities (1, 2, 3 and 4), k is set to be the loss factor. Therefore, the transmission of the proposed metamaterials waveguide is given as follows:

$$T = \left|\frac{S_{2-}}{S_{1+}}\right|^2 = \left| k_{e1}k_{e2} \Big/ \begin{array}{c} [j(\omega-\omega_A) + k_{o1}^2 + k_{e1}^2 + k_{e2}^2 + k_{e3}^2 + k_{e4}^2 + k_{e5}^2] - \\ k_{e3}^2/[j(\omega-\omega_B) + k_{o2}^2 + k_{e3}^2] - k_{e4}^2/[j(\omega-\omega_C) + k_{o3}^2 + k_{e4}^2] - \\ k_{e5}^2/[j(\omega-\omega_D) + k_{o4}^2 + k_{e5}^2] - k_{e6}^2/[j(\omega-\omega_E) + k_{o5}^2 + k_{e6}^2] \end{array} \right|^2 . \quad (12)$$

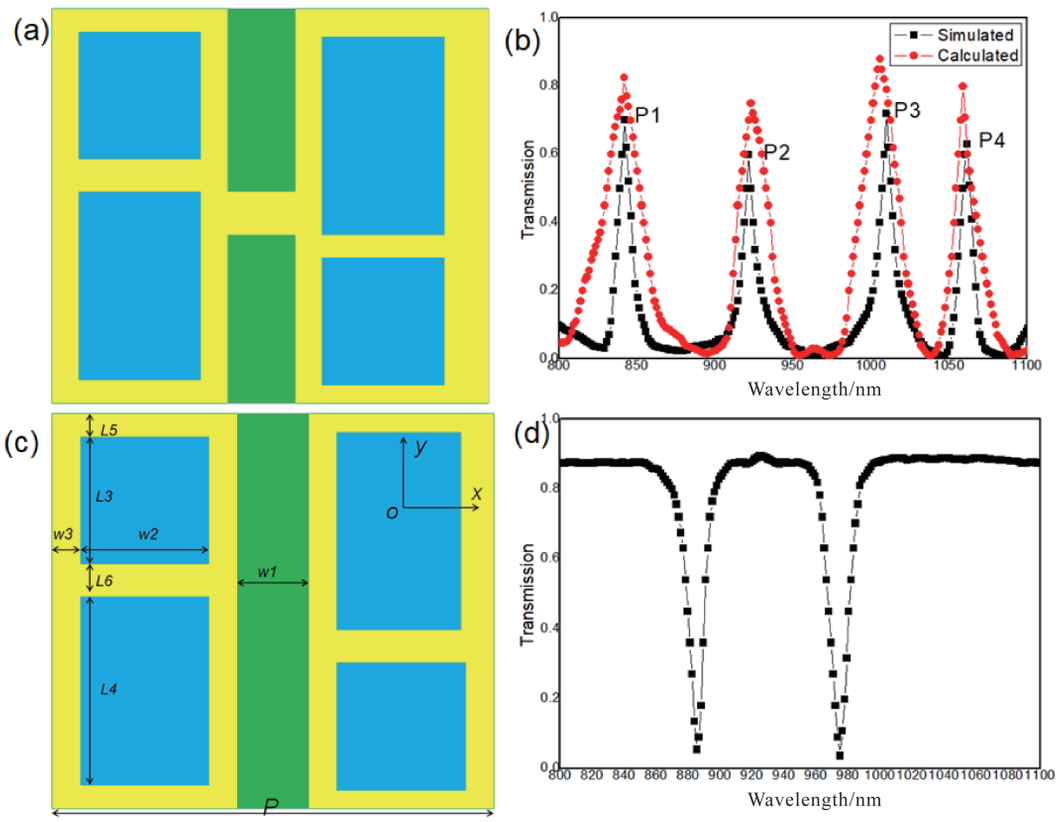

Fig 2　(a) The schematic diagram of the proposed structure. (b) Simulated and calculated transmission spectrum of the proposed structure. (c) Schematic diagram of the waveguide without metal reflector layer. (d) Simulated and calculated transmission spectrum of the waveguide without metal reflector layer

图2　(a)该研究的结构单元示意图(b)该研究的结构单元的仿真透射谱和理论计算透射谱(c)没有中间反射条的结构单元示意图(d)没有中间反射条的结构单元的仿真透射谱

According to the equation above, when the calculated frequency is satisfied as follows:

$$\omega = \omega_A = \omega_B \quad . \quad (13)$$

Then, interference conditions between the main cavity and the Cavity 1 are achieved, which leads to the transmission enhance and the P1. Therefore, when the calculated frequency deviates from the resonance frequency of Cavity 1 ω_B, the transmittance is suppressed, as shown in Fig 2(b) and Fig 3(a).

At the resonance position of the P2, magnetic field intensity is mainly distributed in the main cavity and the Cavity 2, as shown in Fig 3(b). The magnetic field intensity in the cavities 1, 3, and 4 is weekly. Moreover, the phase difference is also close to zero at the resonance position of the P2, as shown in Fig 5. It is revealed that the transmission is enhanced by interference between the main cavity and the Cavity 2, which results in the P2. When the calculated frequency is deviated from the resonance frequency of Cavity 2 ω_C, the interference conditions between the main cavity and the Cavity 2 are failure, the transmission is reduced and the electromagnetic wave energy is blocked by the reflective layer, as shown in Fig 3(d). For the transmission peaks P3 and P4, transmission interference strength phenomenons between the main cavity and the Cavities 3 or 4 are also can be found when the conditions $\omega = \omega_A = \omega_D$ or $\omega = \omega_A = \omega_E$are achieved, as shown in Fig 4 (a-b). Moreover, the phase differences are also close to zero at the resonance position of the P3 or P4, as shown in Fig 5.

The proposed waveguide contains a Dirac semimetal reflector (A short metal bar located in the middle of Dirac semimetal layers), as shown in Fig 2(a). It is obvious that the electromagnetic wave energy is blocked by the Dirac semimetal reflector and can't penetrate the waveguide cavity, as shown in Fig 3(c~d) and Fig 4 (c~d). Therefore, this reflector in the proposed metamaterials waveguide plays a transmission band selector. To reveal the effect of this Dirac semimetal reflector, a waveguide without this reflector is also designed and simulated, as shown in Fig 2(c~d). It is found that two transmission valleys are revealed at resonance wavelengths 885nm and 973nm, respectively, as shown in Fig 2(d). The magnetic field intensity of the waveguide without reflector is achieved in Fig 6. It is found that most of electromagnetic wave energy is travelled along the waveguide cavity in transmission bands, as shown in Fig6 (a~b).

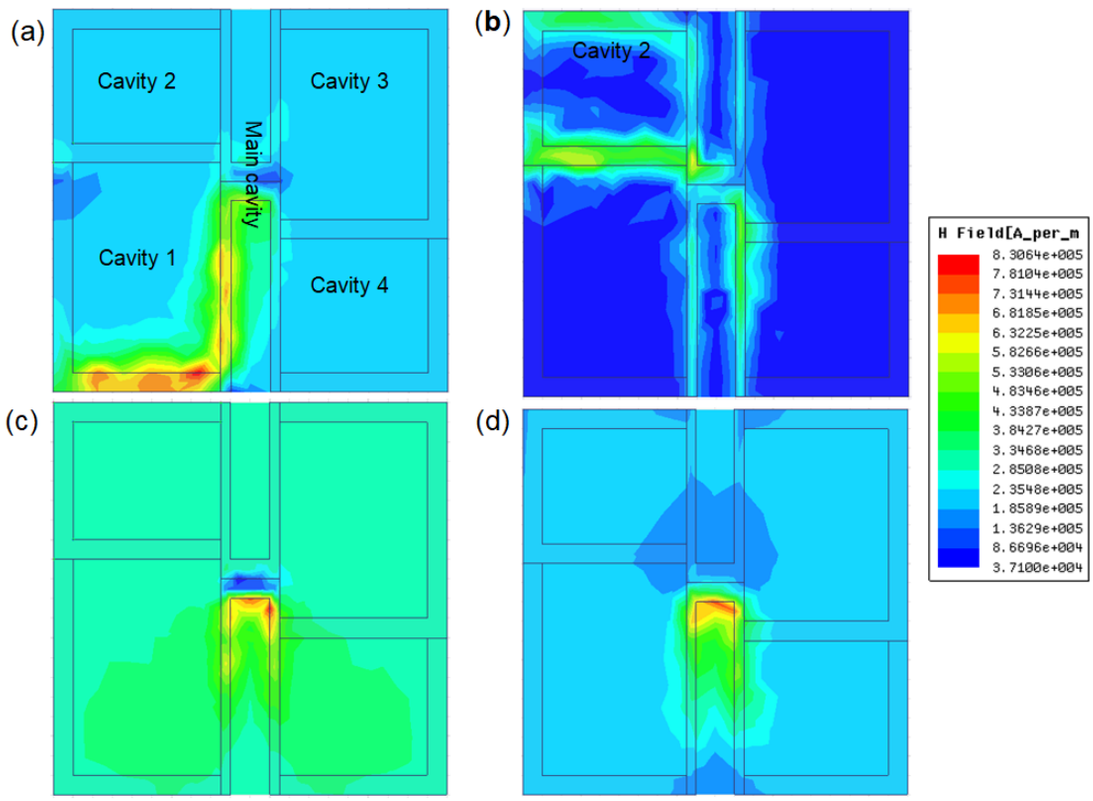

Fig 3 (a) The magnetic field intensity distribution at resonance wavelength 842nm. (b) The magnetic field intensity distribution at resonance wavelength 921nm. (c) The magnetic field intensity distribution at resonance wavelength 900nm. (d) The magnetic field intensity distribution at resonance wavelength 950nm

图3 (a) 磁场共振强度在波长842nm的分布结果 (b) 磁场共振强度在波长921nm的分布结果 (c) 磁场共振强度在波长900nm的分布结果 (d) 磁场共振强度在波长950nm的分布结果

However, electromagnetic wave energy is blocked at the front metal layer the waveguide without reflector, as shown in Fig 6(c-d).

On the one hand, according to Equation (4), it can be known that the dispersion equation of SPP modes is related to the permittivity of the proposed waveguide. On the other hand, the proposed waveguide is made of Dirac semimetal, and the permittivity of this material is sensitive to Fermi energy. Therefore, the resonance properties of the waveguide can be modulated by changing the Fermi energy. To verify the tunability of this waveguide, different Fermi energies are used. The simulated transmission spectrum is shown in Fig 7. The Fermi energy of Dirac semimetal layers is enhanced from 50meV to 70meV. It is found that all of transmission peaks are enhanced. Moreover, these transmission peaks are shifted to lower resonance wavelengths, which confirms the tunable of this proposed waveguide. The real and imaginary parts of the permittivity of Dirac semimetals layers are shown in Fig 8. It is revealed that the real part of the permittivity is reduced with the Fermi energy of Dirac semimetal layers increasing, as shown in Fig 8. The perturbation theory can be used to reveal the relationship between the resonance wavelengths and the permittivity of Dirac semimetals layers [31-33]:

$$\frac{\triangle\omega}{\omega_o}=\frac{\omega-\omega_o}{\omega_o}\approx\frac{-\iiint_V dV\left[(\triangle\vec{\varepsilon}\cdot\vec{E})\cdot\vec{E}_o+(\triangle\vec{\mu}\cdot\vec{H})\cdot\vec{H}_o^*\right]}{\iiint dV\left(\varepsilon\left|\vec{E}_o\right|^2+\mu\left|\vec{H}_o\right|^2\right)} \quad (14)$$

Based on the simulated results in Fig 8, as the Fermi energy increasing, the real part of the dielectric constant is reduced, which results in the $\triangle\vec{\varepsilon}$is lower than zero. According to the equation (14), the resonance frequency is enhanced (resonance wavelength is shifted to shorter wavelengths) due to the $\triangle\vec{\varepsilon}$is lower than zero, as shown in Fig 7. It should be noted that these transmission peaks cannot achieve perfect transmission, as shown in Figures 2 and 7, mainly due to the high imaginary part of the permittivity of Dirac semimetals, which leads to the inevitable energy loss of electromagnetic waves. However, the permittivity of the Dirac semimetal is sensitive to Fermi energy, as shown in Fig 7. Therefore, this material can be used to design and develop a tunable metamaterial waveguide. At the same time, simulation results also show that the transmittance of this tunable metamaterial waveguide can be enhanced by adjusting Fermi energy, as shown in Figure 7.

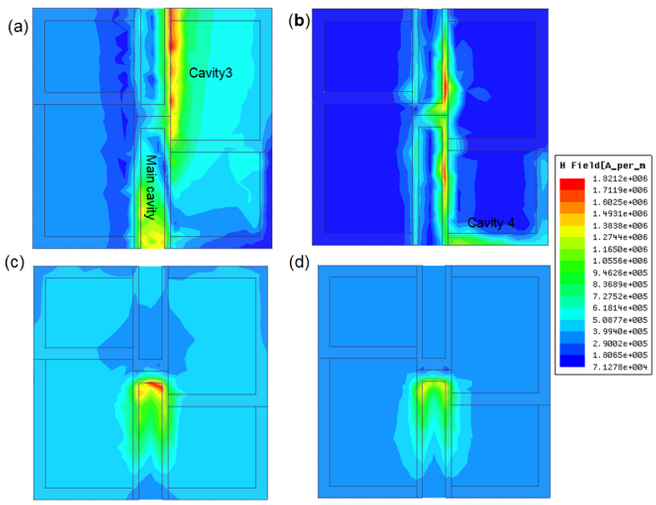

Fig 4　(a) The magnetic field intensity distribution at resonance wavelength 1010nm. (b) The magnetic field intensity distribution at resonance wavelength 1061nm. (c) The magnetic field intensity distribution at resonance wavelength 1040nm. (d) The magnetic field intensity distribution at resonance wavelength 1080nm

图 4　(a) 磁场共振强度在波长 1010nm 的分布结果 (b) 磁场共振强度在波长 1061nm 的分布结果 (c) 磁场共振强度在波长 1040nm 的分布结果 (d) 磁场共振强度在波长 1080nm 的分布结果

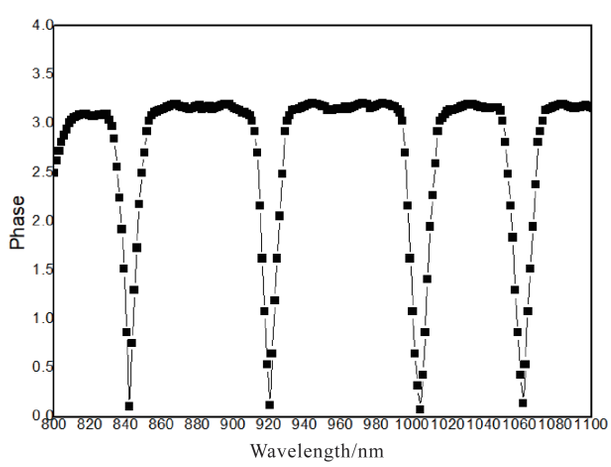

Fig 5　The phase spectrum of the proposed structure

图 5　该研究的结构单元的相谱

3　Conclusion

In conclusion, a tunable metamaterial waveguide is numerically investigated with Dirac semimetal layers. Four transmission peaks (70%, 61%, 72%, and 63%) are achieved in the 800~1100nm range. Simulated results reveal that these transmission peaks are originated from the interference effect between the main cavity and the Cavities 1, 2, 3, or 4. Four transmission peaks can be tuned through changing the Fermi energy. The proposed metamaterial waveguide may have application in nanoscale filter, switch, or refractive index sensor.

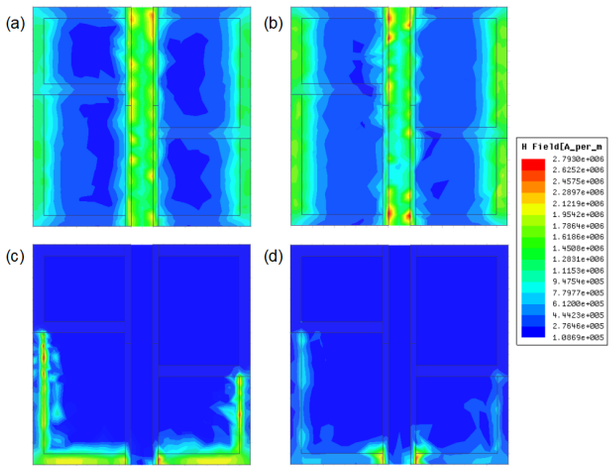

Fig 6　(a) The magnetic field intensity distribution of the waveguide without metal reflector layer at resonance wavelength 840nm. (b) The magnetic field intensity distribution of the waveguide without metal reflector layer at resonance wavelength 940nm. (c) The magnetic field intensity distribution of the waveguide without metal reflector layer at resonance wavelength 885nm. (d) The magnetic field intensity distribution of the waveguide without metal reflector layer at resonance wavelength 973nm

图 6　(a) 没有中间反射条的结构单元的磁场共振强度在波长 840nm 的分布结果 (b) 没有中间反射条的结构单元的磁场共振强度在波长 940nm 的分布结果 (c) 没有中间反射条的结构单元的磁场共振强度在波长 885nm 的分布结果 (d) 没有中间反射条的结构单元的磁场共振强度在波长 973nm 的分布结果

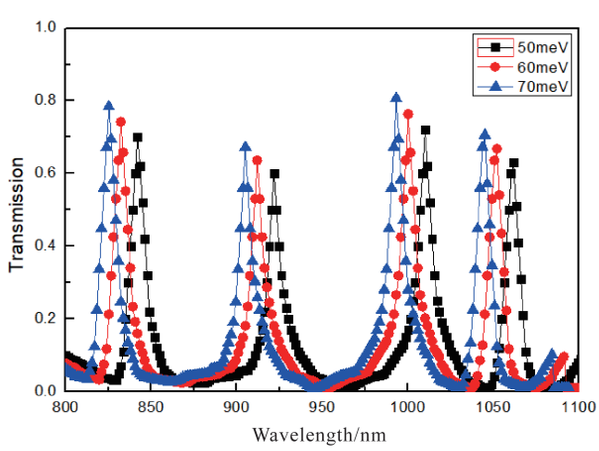

Fig 7　Transmission spectrum with different Fermi energy

图 7　不同费米能级条件下的透射谱

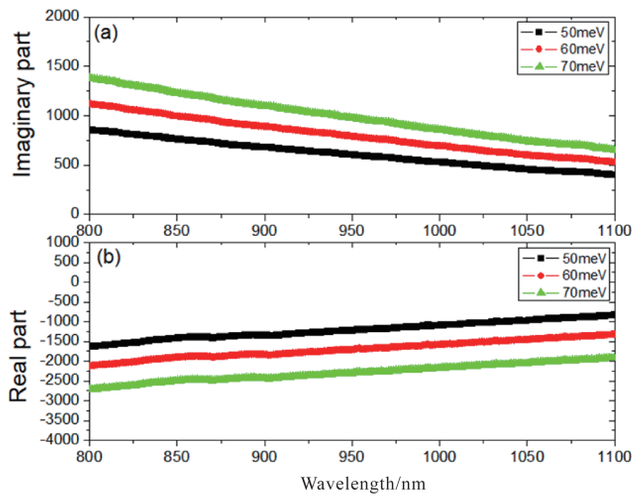

Fig 8 (a) Imaginary parts of the permittivity of Dirac semimetals layers. (b) Real parts of the permittivity of Dirac semimetals layers

图8 (a)狄拉克半金属的介电常数的虚部(b)狄拉克半金属的介电常数的实部

References

[1] Liu C, Liu P, Yang C, *et al*. Analogue of dual-controlled electromagnetically induced transparency based on graphene metamaterial [J]. *Carbon*, 2019, **142**:354 - 362.

[2] Smith D R, Pendry J B, Wiltshire M C K, Metamaterials and negative refractive index [J]. *Science*, 2004, **305**:788 - 792 .

[3] He X, Yao Y, Yang X, *et al*. Dynamically controlled electromagnetically induced transparency in terahertz graphene metamaterial for modulation and slow light applications [J]. *Opt. Commun*, 2018, **410**:206 - 210 .

[4] Badioli M, Woessner A, Tielrooij K J, *et al*. Phonon-mediated mid-Infrared photoresponse of grapheme [J]. *Nano Lett*, 2014, **14** (11) : 6374 - 6381.

[5] Liang T, Gibson Q, Ali M, *et al*. Ultrahigh mobility and giant magnetoresistance in the Dirac semimetal Cd3As2 [J]. *Nat. Mater*, 2015,**14** (3): 280 - 284.

[6] Zhong S M, He S L, Ultrathin and lightweight microwave absorbers made of mu-near-zero metamaterials, SCIENTIFIC REPORTS, 2013,**3** : 2083- 2087.

[7] Yong Z D, Zhang S L, Gong C S, *et al*. Narrow band perfect absorber for maximum localized magnetic and electric field enhancement and sensing applications [J]. *Scientific Reports*, 2016, **6**: 24063-24069.

[8] Mei J, Ma G C, Yang M, *et al*. Dark acoustic metamaterials as super absorbers for low-frequency sound [J]. *Nature communications* , 2011,**3**:756-762.

[9] Zhang Y P, Li T T, Chen Q, *et al*. Independently tunable dualband perfect absorber based on graphene at mid-infrared frequencies [J]. *Scientific Reports*, 2015,**5**:18463-18470.

[10] Cao G T, Li H J, Zhan S P, *et al*. Uniformtheoretical description of plasmon-induced transparency in plasmonic stubwaveguide [J]. *Opt. Lett*, 2014, **39**:216 - 219.

[11] Deng Y, Cao G T, Wu Y W, *et al*. Theoretical description of dynamic transmission characteristics in MDM waveguide aperture-side-coupled with ring cavity [J]. *Plasmonics*, 2015, **10** :1537 - 1543.

[12] Lai G, Liang R S, Zhang Y J, *et al*. Doubleplasmonic nanodisks design for electromagnetically induced transparencyand slow light [J]. *Opt. Express*, 2015, **23**: 6554 - 6561.

[13] He Z, Li H, Li B, *et al*. Theoretical analysis of ultrahighfigure of merit sensing in plasmonic waveguides with a multimode stub [J]. *Opt.Lett*, 2016, **41**:5206 - 5209.

[14] Huang Y, Min C J, Veronis G. Broadband near total light absorption innon-PT-symmetric waveguide-cavity systems [J]. *Opt. Express*, 2016, **24**:22219 - 22231.

[15] Chen L, Liu Y M, Yu Z Y, *et al*. Numerical analysis of anear-infrared plasmonic refractive index sensor with high figure of meritbased on a fillet cavity [J]. *Opt. Express*, 2016, **24**: 9975 - 9983.

[16] Yankovich A B, Verre R, Olsén E, *et al*. Electron-Energy Loss Study of Nonlocal Effects in Connected Plasmonic Nanoprisms [J]. *ACS Nano*, 2017, **11**:4265-4274.

[17] Zeng C, Cui Y D. Rainbow trapping of surface plasmon polariton waves in metal-insulator-metal graded grating waveguide [J]. *Opt Commun*, 2013, **290**(1): 188-191.

[18] Huang L L, Chen X Z, Bai B F, *et al*. Dependent Directional Surface Plasmon Polariton Excitation Using A Metasurface with Interfacial Phase Discontinuity[J]. *Light-Sci. Appl*. 2013,**2**:70-76.

[19] Fu H X, Li S L, Wang Y, L*et al*. Generation of polarization-locked vector solitons in mode-locked thulium fiber laser[J]. *IEEE Photonics J*,2018, **10**: 1500308- 1500316

[20] Li S L, Wang Y L, Jiao R Z, *et al*. Fano resonances based on multimode and degenerate mode interference in plasmonic[J]. *Opt. Exp*, 2017, **25**:3525 - 3533.

[21] Chen Z, Yu L, Multiple Fano Resonances Based on Different Waveguide Modes in a Symmetry Breaking Plasmonic System [J]. *IEEE Photonics J*,2014, **6**:1-8

[22] Li C, Li S L, Wang Y L, *et al*. Multiple Fano Resonances Based on Plasmonic Resonator System With End-Coupled Cavities for High-Performance Nanosensor[J], *IEEE Photonics J*, 2017, **9**:1-9

[23] Wang Q, Ouyang Z B, Lin M, *et al*. Independently tunable Fano resonance based on the coupled hetero cavities in a plasmonic MIM system[J]. *Materials*, 2018, **11**:1675-1684.

[24] Zheng G, Zhang H, Bu L, *et al*. Tunable Fano resonances in midinfrared waveguide-coupled otto configuration[J]. *Plasmonics*, 2018, **13** (1) : 215 - 220

[25] Yia X C, Tiana J P, Yanga R C,Tunable Fano resonance in plasmonic MDM waveguide with a square type split-ring resonator[J]. *Optik - International Journal for Light and Electron Optics*, 2018, **171** : 139 - 148

[26] Kotov O V, Lozovik Y E, Dielectric response and novel electromagnetic modes in three-dimensional Dirac semimetal films[J]. *Phys. Rev*. B, 2016, **93**:235417.

[27] Timusk T, Carbotte J P, Homes C C, *et al*. Three-dimensional Dirac fermions in quasicrystals as seen via optical conductivity [J]. *Phys. Rev*. B,2013, **87**:235121.

[28] Zand I, Mahigir A, Pakizeh T, *et al*. Selective-mode optical nanofilters based on plasmonic complementary split-ring resonators[J].*Opt. Express*, 2012,**20** (7) : 7516 - 7525.

[29] Smith D R, Schult S, Markos P, *et al*. Determination of effective permittivity and permeability of metamaterials from reflection and transmission coefficients[J]. *Phys.Rev. B*,2002, **65**: 195104 - 195108.

[30] Piao X J, Yu S, Koo S, *et al*. Fano-type spectral asymmetry and its control for plasmonic metal-insulator-metal stub structures [J].*Opt. Express* ,2001,**19** :10907-10912.

[31] Yao Y, Kats M A, Genevet P, *et al*. Broad electrical tuning of graphenеloaded plasmonic antennas[J]. *Nano Lett*,2013, **13**: 1257 - 1264.

[32] Li Z, Yu N, Modulation of mid-infrared light using graphene-metal plasmonic antennas[J]. *Appl. Phys. Lett*, 2013,**102**(13):131108.

[33] Hwang J, Roh J W, Electrically tunable two-dimensional metasurfaces at near-infrared wavelengths[J]. *Opt.Express*, 2017, **25**(21): 25071 - 25078.